JCEC
THE JOURNAL OF ENGINEERING AND EXACT SCIENCES

OPEN ACCESS

The Journal of Engineering and Exact Sciences – jCEC, Vol. 10 N. 09 (2024)
journal homepage: https://periodicos.ufv.br/jcec
eISSN: 2527-1075
ISSN: 2446-9416

Passivity Based Control of Doubly Fed Induction Generator Using an Interval Type-2 Fuzzy Logic Controller

Article Info:
Article history: Received 2024-11-15 / Accepted 2024-12-20 / Available online 2024-12-23
doi: 10.18540/jcecvl10iss9pp21012

Izzeddine Allali
ORCID: https://orcid.org/0009-0006-3668-7336
IRECOM-laboratory, University DjillaliLiabes of SidiBel-Abbes,
BP 89 SidiBel Abbes 22000-Algeria,
E-mail: izzeddine.allali@univ-sba.dz
Boubekeur Dehiba
ORCID: https://orcid.org/0000-0002-0175-0140
IRECOM-laboratory, University DjillaliLiabes of SidiBel-Abbes,
BP 89 SidiBel Abbes 22000-Algeria,
E-mail: deh_mas@yahoo.fr

Abstract.
The article is interested in the control of a Doubly Fed Induction Generator (DFIG) for wind energy conversion. The proposed structure is based on the association of passivity and interval type 2 fuzzy logic control. The principal objective of this task is to effectively regulate and optimize the flow of both active and reactive power from the generator to the interconnected network to ensure efficient operation and stability, with the rotor signals operated via a bidirectional converter. The proposed control technique is subjected to various conditions to evaluate its performance, including varying wind speeds and parameter adjustments. The simulation results show the robustness of the proposed control, where the integration of the interval type 2 fuzzy logic controller (IT2-FLC) enhances the dynamic performance, disturbance sensitivity, and robustness against parameter changes.
Keywords: Doubly fed induction generator, Wind power, Passivity based control, Interval type-2 fuzzy logic control.

Introduction

Wind energy has experienced significant growth over the past decade due to its ability to be both sustainable and environmentally beneficial (Xiong *et al*., 2021; Heier, 2014). Due to diminishing fuel supplies, conventional power generation has become more expensive. Increased public awareness of environmental issues associated with thermal and nuclear power has led to greater interest in wind power generation systems (WPGS) as a leading renewable energy solution. Worldwide, wind power capacity has surpassed the gig watt (GW) threshold, and larger wind power plants are planned (Yin *et al*., 2016; Scarabaggio *et al*., 2021).

Currently, the majority of wind turbines have a DFIG installed because of its many benefits: variable speed production (with a ± 30% variation around the synchronous speed), separated control over active and reactive power (Ps and Qs), less noise and mechanical stress, enhanced power quality, and cheap cost (Khan *et al*., 2020).

The control of the Doubly Fed Induction Machine (DFIM) based system necessitates applying classical methods, including proportional, integral, and derivative action. A thorough understanding of all system parameters and the ability to respond accordingly is essential to implement this control strategy successfully. However, errors and a lack of precision in this knowledge often occur. Furthermore, the interconnected nature of the system's variables adds

complexity to the control process (Kaloi *et al*., 2019). This problem can be solved using non-linear techniques, such as sliding mode (Amira *et al*., 2020), integral backstepping control (Doumi *et al*., 2016), SIDA-PBC control (Hichem *et al.*, 2023), and fuzzy logic (Hemeyine *et al.*, 2020).

The primary drawback of these directives lies in their reliance on a rigorous mathematical approach. In contrast, orders such as passive control offer more physically meaningful alternatives (Belkhier *et al.*, 2022).

Due to its simplicity and common application in mechanical, electrical, and electromechanical systems, passive-based control (PBC) has become a key method for nonlinear control (Minka et al., 2019; Hichem *et al.*, 2023). A significant advantage of PBC, also known as energy-based control (EBC), is its ability to manage nonlinear characteristics rather than eliminate them. PBC designs primarily focus on redistributing the system's inherent energy and adding necessary damping to meet regulatory goals. By preserving system nonlinearities, this approach enhances resilience and avoids the complexities associated with discontinuous controller computations (Minka *et al*., 2019; Saihi *et al*., 2023).

The proposed integrated control system combines interval type-2 fuzzy logic control and IDA-PBC to mitigate coupling effects, parametric uncertainties, and speed variations. The fundamental principle of IDA-PBC is a method for controlling nonlinear systems by imposing a specific port-controlled Hamiltonian (PCH) structure on the closed loop. The main challenge is identifying the process model's workless force terms that do not impact its dynamics (Sanjuan *et al.*, 2018; Yang *et al.*, 2018).

Professor Zadeh first put out the fuzzy theory in 1965. A steam engine and boiler system were controlled using linguistic rules by using the Mamdani fuzzy inference system. Fuzzy logic makes use of natural language when expressing if-then rules (Hemeyine *et al.*, 2020).

Fuzzy logic type-1, also known as classical fuzzy logic, has been expanded and evolved into a more advanced form called fuzzy logic type-2. During the last few years, numerous researchers have dedicated their efforts to studying this emerging form of fuzzy logic (Kheir Saadaoui *et al.*, 2019), and have established the necessary theoretical groundwork (Acikgoz *et al.*, 2017; Yan *et al.*, 2024).

This paper is organized as follows: First, the modeling of the conversion system is discussed, followed by the presentation of the proposed Passivity-Fuzzy Logic Controller (PFLC) method for active and reactive power control. It then provides a comprehensive analysis of the results and concludes with a summary and conclusions.

Modeling the conversion system

The wind conversion system is shown in Figure 1.

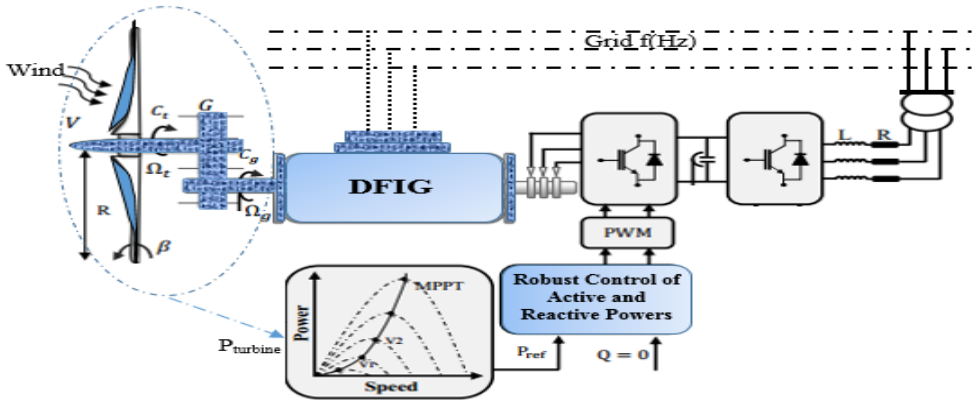

Figure 1 - Synoptic diagram of the wind system.

Modeling the turbine

The equation illustrates the wind speed (v) and turbine energy recovery from wind kinetic energy (P_m) (Sahri *et al.*, 2021; Shuaibu *et al.*, 2021).

$$P_m = \frac{1}{2}\rho\pi R^2 v^3 C_p(\lambda,\beta) \quad (1)$$

The wind turbine (WT) blade is represented by R, and the power coefficient C_p is determined by the tip speed ratio λ, provided by the equation.

$$\lambda = \frac{\Omega.R}{v} \quad (2)$$

The angular speed of the turbine rotor is denoted by Ω. Theoretically, the power coefficient C_p cannot exceed 0.593 (Adeyanju, 2023). Turbine torque is the ratio of transmitted power and rotor speed Ω (Sahri *et al.*, 2021; Shuaibu *et al.*, 2021):

$$T_m = \frac{P_m}{\Omega} = \frac{1}{2\lambda}\rho\pi R^3 v^2 C_p(\lambda,\beta) \quad (3)$$

The power coefficient C_p varies with the pitch angle β and the tip speed ratio λ (Milles *et al.*, 2024; Okedu. *et al.*, 2021)

$$C_p(\lambda,\beta) = c_1\left(\frac{c_2}{\lambda_i} - c_3\beta - c_4\right)e^{-\frac{c_5}{\lambda_i}} + c_6\lambda \quad (4)$$

With: c_1= 0.5176, c_2 = 116, c_3 = 0.4, c_4 = 5, c_5 = 21, c_6 = 0.0068.

Where λ_i is given by the equation (Milles *et al.*, 2024; Okedu. *et al.*, 2021):

$$\lambda_i = \left[\frac{1}{(\lambda+0.08\beta)} - \frac{0.35}{(\beta^3+1)}\right]^{-1} \quad (5)$$

Optimizing wind turbine efficiency relies on maximum power point tracking (MPPT) control to regulate speed, especially at low wind speeds. This is achieved by maintaining the optimal values of λ_{opt} = 8.1, assuming β = 0 (Sahri *et al.*, 2021; Hemeyine *et al.*, 2020), to obtain the maximum power coefficient C_{p-max}. The electromagnetic torque Tem of the DFIG turbine must be regulated to maintain the DFIG speed at the reference speed (Mousa *et al.*, 2020; Kadri *et al.*, 2020).

$$T_m = \frac{\rho}{2}\frac{c_{p-max}}{\lambda_{opt}^3}\pi\frac{R_t^5}{G}\Omega_{mec}^2 \quad (6)$$

Excessive wind speed can damage the turbine structure, so the speed must be limited to the rated speed. The pitch controller must monitor the power output of the wind turbine and adjust the blade pitch to optimize performance across varying wind speeds (Mousa *et al.*, 2020; Hemeyine *et al.*, 2020).

Modeling of the DFIG

The following equations characterize the DFIG model in the d-q reference frame (Hemeyine *et al.*, 2020).

$$\begin{cases} V_{sd} = R_s I_{sd} + \frac{d\phi_{sd}}{dt} - \omega_s\phi_{sq} \\ V_{sq} = R_s I_{sq} + \frac{d\phi_{sq}}{dt} + (\omega_s - \omega_r)\phi_{sd} \\ V_{rd} = R_r I_{rd} + \frac{d\phi_{rd}}{dt} - \omega_s\phi_{rq} \\ V_{rq} = R_r I_{rq} + \frac{d\phi_{rq}}{dt} + (\omega_s - \omega_r)\phi_{rd} \end{cases} \quad (7)$$

Rotor and stator fluxes are expressed as follows.

$$\begin{cases} \phi_{sd} = L_s I_{sd} + M I_{rd} \\ \phi_{sq} = L_s I_{sq} + M I_{rq} \\ \phi_{rd} = L_r I_{rd} + M I_{sd} \\ \phi_{rq} = L_r I_{rq} + M I_{sq} \end{cases} \quad (8)$$

The mechanical equation of the system is

$$\Gamma_{em} = \Gamma_r + C_f \Omega_{mec} + J_T \frac{d\Omega_{mec}}{dt} \quad (9)$$

Torque can be expressed as:

$$\Gamma_{em} = p \frac{M}{L_s} (\phi_{sd} I_{rq} - \phi_{sq} I_{rd}) \quad (10)$$

The DFIG powers are defined as:

$$\begin{cases} P_s = V_{sd} I_{sd} + V_{sq} I_{sq} \\ Q_s = V_{sq} I_{sd} - V_{sd} I_{sq} \end{cases} \quad (11)$$

IDA-PBC controller applied to DFIG generator

The DFIG's dynamic model is non-linear due to the interplay between electric currents and speed. When the direct axis current I_d is set to zero, the vector control concept aligns all linkage flux along the d-axis, maximizing torque per ampere.

$$\begin{cases} \frac{d\phi_{sd}}{dt} = V_{sd} - R_s I_{sd} + \omega_s L_s I_{sq} + \omega_s M I_{rq} \\ \frac{d\phi_{sq}}{dt} = V_{sq} - R_s I_{sq} - \omega_s L_s I_{sd} - \omega_s M I_{rd} \\ \frac{d\phi_{rd}}{dt} = V_{rd} - R_r I_{rd} + \omega_r L_r I_{rq} + \omega_r M I_{sq} \\ \frac{d\phi_{rq}}{dt} = V_{rq} - R_s I_{rq} - \omega_r L_r I_{rd} + \omega_r M I_{sd} \end{cases} \quad (12)$$

The generator's spinning component's mechanical equation is thus:

$$J \frac{d\omega}{dt} = M I_S^T J_2 I_r - T_r - T_f \quad (13)$$

Where: $J_2 = \begin{bmatrix} 0 & -1 \\ 1 & 0 \end{bmatrix}, I_s = \begin{bmatrix} I_{sd} \\ I_{sq} \end{bmatrix}, I_r = \begin{bmatrix} I_{rd} \\ I_{rq} \end{bmatrix}$

The state variables are:

$x = [\phi_s^T \phi_r^T J\omega\ ]^T = [x_e^T x_m\ ]^T$

With:

$x_e^T = [\phi_s^T \phi_r^T]$: are the electrical state variables.

$x_m = J\omega$: mechanical variable.

The energy function is written as:

$$H(x) = \frac{1}{2} x_e^T L^{-1} x_e + \frac{1}{2 J_{DFIG}} x_m^2 \quad (14)$$

With: $L = \begin{bmatrix} L_s I_2 & M I_2 \\ M I_2 & L_r I_2 \end{bmatrix}, I_2 = \begin{bmatrix} 1 & 0 \\ 0 & 1 \end{bmatrix}$

Regarding state variables, the partial derivatives of energy are:

$$\begin{cases} \frac{\partial H}{\partial x_e} = L^{-1} x_e \\ \frac{\partial H}{\partial x_m} = J^{-1} x_m \end{cases} \Rightarrow \begin{cases} \frac{\partial H}{\partial x_e} = I = [I_s^T I_r^T]^T \\ \frac{\partial H}{\partial x_m} = \omega \end{cases} \quad (15)$$

Finally, the following are the matrices representing the command, damping, and interconnection:

$$J(x) = \begin{bmatrix} -\omega_s L_s J_2 & -\omega_s M J_2 & 0_{2\times1} \\ -\omega_s L_s J_2 & -\omega_r L_s J_2 & M J_2 I_s \\ 0_{1\times2} & M I_S^T J_2 & 0 \end{bmatrix}, R(x) = \begin{bmatrix} R_s I_2 & 0_{2\times2} & 0_{2\times1} \\ 0_{2\times2} & R_r I_2 & 0_{2\times1} \\ 0_{1\times2} & 0_{1\times2} & T_f \end{bmatrix} \quad (16)$$

$$g(x) = \begin{bmatrix} I_2 & 0_{2\times2} & 0_{2\times1} \\ 0_{2\times2} & I_2 & 0_{2\times1} \\ 0_{1\times2} & 0_{1\times2} & 1 \end{bmatrix}, u = [V_s^T \quad V_r^T \quad T_r]^T \quad (17)$$

With:

$0_{2\times2} = \begin{bmatrix}0 & 0\\ 0 & 0\end{bmatrix}, 0_{2\times1} = \begin{bmatrix}0\\ 0\end{bmatrix}, 0_{1\times2} = [0\ 0], V_s^T = \begin{bmatrix}V_{sd}\\ V_{sq}\end{bmatrix} V_r^T = \begin{bmatrix}V_{rd}\\ V_{rq}\end{bmatrix}$

$J(x) = J(x)^{-1}, R(x) = R(x)^T \geq 0$

(18)

The PCH model may be expressed using these matrices:

$$\dot{x} = \left[\begin{bmatrix}-\omega_s L_s J_2 & -\omega_s M J_2 & 0_{2\times1}\\ -\omega_s M J_2 & -\omega_r L_s J_2 & M J_2 I_s\\ 0_{1\times2} & M I_S^T J_2 & 0\end{bmatrix} - \begin{bmatrix}R_s I_2 & 0_{2\times2} & 0_{2\times1}\\ 0_{2\times2} & R_r I_2 & 0_{2\times1}\\ 0_{1\times2} & 0_{1\times2} & T_f\end{bmatrix}\right] \nabla H + \begin{bmatrix}I_2 & 0_{2\times2} & 0_{2\times1}\\ 0_{2\times2} & I_2 & 0_{2\times1}\\ 0_{1\times2} & 0_{1\times2} & 1\end{bmatrix}\begin{bmatrix}V_s^T\\ V_r^T\\ T_r\end{bmatrix} \quad (19)$$

$$\dot{y} = \begin{bmatrix}I_2 & 0_{2\times2} & 0_{2\times1}\\ 0_{2\times2} & I_2 & 0_{2\times1}\\ 0_{1\times2} & 0_{1\times2} & 1\end{bmatrix}\nabla H \quad (20)$$

Calculation of control voltages V_{dr}, V_{qr}

Finding $J_d(x)$ and $R_d(x)$ is necessary to calculate the control voltages.

To obtain the controller's $J_d(x)$ and $R_d(x)$, the closed-loop system can be written as:

$$f(x) + g(x)u = \big(J_d(x) - R_d(x)\big)\partial H_d(x) \quad (21)$$

Where:

$$J_d(x) = J(x) + J_a(x)$$
$$R_d(x) = R(x) + R_a(x) \quad (22)$$
$$H_d(x) = H(x) + H_a(x)$$

$H_d(x)$: The closed-loop system's energy function.

$J_d(x)$: The closed-loop system's connectivity matrix.

$R_d(x)$: The closed-loop system's damping matrix, as given in Equation (21), can be expressed as:

$$\big(J(x) + J_a(x) - R(x) + R_a(x)\big)\partial H_d(x) = -\big(J_a(x) - R_a(x)\big)\partial H(x) + g(x)u \quad (23)$$

Equation (23) is equivalent to:

$$\big(J_d(x) - R_d(x)\big)\partial H_a(x) = -\big(J_a(x) - R_a(x)\big)\partial H(x) + g(x)u \quad (24)$$

So, the desired total energy:

$$H_d(x) = \frac{1}{2}(x_e - x_e^*)^T L^{-1}(x_e - x_e^*) + \frac{1}{2J_{DFIG}}(x_m - x_m^*)^2 \quad (25)$$

So:

$$H_a(x) = H_d(x) - H(x) = -x_e^T L^{-1} x_e - \frac{1}{J_{DFIG}} x_m^* x_m + \frac{1}{2} x_e^{*T} L^{-1} x_e^* + \frac{1}{2J_{DFIG}} x_e^{*2} \quad (26)$$

With:

$$\partial H_a(x) = \begin{bmatrix}-I^*\\ -\omega^*\end{bmatrix}, \text{where } I = [I_{sd} I_{sq} I_{rd} I_{rq}]^T$$

By employing this relationship, (21) is transformed into:

$$\big(J_d(x) - R_d(x)\big)\begin{bmatrix}-I^*\\ -\omega^*\end{bmatrix} = -\big(J_a(x) - R_a(x)\big)\begin{bmatrix}I\\ \omega\end{bmatrix} + g(x)u \quad (27)$$

Lines 3 and 4 of the matrix in (27) contain the command V_r. So:

$$J_a(x) = \begin{bmatrix}0_{2\times2} & 0_{2\times2} & 0_{2\times1}\\ 0_{2\times2} & 0_{2\times2} & -J_{rm}(x)\\ 0_{1\times2} & J_{rm}^T(x) & 0\end{bmatrix}, R_a(x) = \begin{bmatrix}0_{2\times2} & 0_{2\times2} & 0_{2\times1}\\ 0_{2\times2} & rI_2 & 0_{2\times1}\\ 0_{1\times2} & 0_{1\times2} & 0\end{bmatrix} \quad (28)$$

Where:

$J_{rm}^T(x) \in \Re^{2\times1}$ to be determined.

r: This extra resistance acts as a dampener for transitory oscillations caused by currents. Substituting $J_a(x)$ and $R_a(x)$ matrices, we use (26) to establish:

$$J_{rm}^T(x) = M\frac{(I_r - I_r^*)^T}{|I_r - I_r^*|^2}(I_s - I_s^*)^T J_2 I_r^* \quad (29)$$

So :

$$V_r = V_r^* - (\omega - \omega^*)(L_r J_2 I_r^* + J_{rm}(x)) - M\omega^* J_2(I_s - I_s^*) - rI_2(I_r - I_r^*) \quad (30)$$

Regrettably, the order is unique at the equilibrium point. By including a variable depreciation, this singularity can be eliminated. Maintaining $J_d(x)$ and $H_d(x)$ unchanged, we now modify the R_a matrix to the following form:

$$R_a(x) = \begin{bmatrix} 0_{2\times2} & 0_{2\times2} & 0_{2\times1} \\ 0_{2\times2} & rI_2 & 0_{2\times1} \\ 0_{1\times2} & 0_{1\times2} & \xi(x) \end{bmatrix} \quad (31)$$

With:

$$\xi(x) = \frac{T_{em}^* - T_{em}(x_e)}{\omega - \omega^*} \quad (32)$$

And:

$$T_{em}^* = C_f\omega^* \quad (33)$$

The closed-loop Hamiltonian equation eliminates singularity by multiplying $\xi(x)$ by $(\omega - \omega^*)$. Because the only portion that has changed in equation (23) is the mechanical part, the formulation of V_r in terms of $J_{rm}(x)$ remains unchanged.

By using the equations for the equilibrium point, we can deduce:

$$J_{rm}(x) = MJ_2 I_s \quad (34)$$

The form (19) is always used by the closed-loop dynamic system, which includes:

$$J_d(x) = \begin{bmatrix} -\omega_s L_s J_2 & -\omega_s M J_2 & 0_{2\times1} \\ -\omega_s L_s J_2 & -\omega_r L_s J_2 & MJ_2 I_s \\ 0_{1\times2} & MI_S^T J_2 & 0 \end{bmatrix}; R_d(x) = \begin{bmatrix} R_s I_2 & 0_{2\times2} & 0_{2\times1} \\ 0_{2\times2} & (R_r + r)I_2 & 0_{2\times1} \\ 0_{1\times2} & 0_{1\times2} & T_f + \xi(x) \end{bmatrix} \quad (35)$$

Finally, the order's rotor voltages are expressed as follows.

$$V_r = V_r^* - (\omega - \omega^*)(L_r J_2 I_r^* + MJ_2 I_s) - M\omega^* J_2(I_s - I_s^*) - rI_2(I_r - I_r^*) \quad (36)$$

With:

$$V_r^* = (\omega_s - \omega^*)(L_r J_2 I_r^* + MJ_2 I_s^*) + R_r I_2 I_r^* \quad (37)$$

Context of fuzzy logic sets

Type-2 fuzzy sets (T2-FSs) offer an enhanced approach for representing imprecision and uncertainty. In 1975, Zadeh introduced the concept of "fuzzy fuzzy" sets, which are characterized by their degree of fuzziness, represented by a type-1 fuzzy set (T1-FS) (Wu and Mendel, 2019). Mendel and Liang (Liang and Mendel, 2000) have introduced innovative concepts for constructing T2-FSs that incorporate superior and inferior membership functions (MFs). Both of these functions can be represented by a T1-FS membership function. The footprint of uncertainty (FOU) refers to the area bounded by these functions delineating T2-FSs.

Different types of reduction processes are one of the main distinguishing characteristics of IT2-FLC compared toT1-FLC (Wu and Mendel, 2019).

Members of Type-1 and Type-2 triangles are displayed in Figure 2. The following is one way to describe the Type-1 MF (Figure 2 (a)):

$$A = (x, \mu_A(x)) \mid x \in X \quad (38)$$

Where $\mu_A(x)$ ranges from 0 to 1, denoting the A set-related variable x membership level. Each variable x has a membership level between 0 and 1, making it impossible to represent the uncertainty. The type-2 MF must be employed when the degree of membership of a variable is not entirely known and cannot be ascertained (Wu and Mendel, 2019).

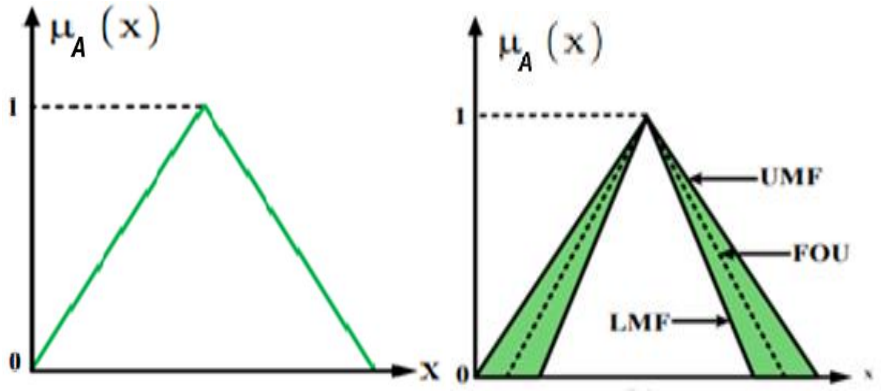

(a) **(b)**

Figure 2 - (a) Type-1 MF, (b) Type-2MF.

The following equations explain the T2-FS shown in Figure 2 (b) and allow its expression (Milles *et al*., 2024):

$\tilde{A}=\{(x,u, (\mu_{\tilde{A}}(x,u))\} \mid \forall_x \epsilon X, \forall_u \epsilon J_x^u \subseteq [0,1]$ (39)

$\tilde{A} = \int_{x\in X} \int_{u\in J_x} 1/\mu_{\tilde{A}}(x,u) J_x \subseteq [0,1]$ (40)

When J_x is a real number between 0 and 1, the union of all valid values of *x* and *u* is shown by the double integral.

The uncertainty about (Ã), represented by the Fou of (Ã), is the sum of all the primary memberships, as illustrated in Figure 2. (b) (Li *et al*., 2023; Magaji *et al*., 2022).

$FOU\ (\tilde{A}) = \cup_{\forall x\in X} J_x = \{(x,u); u\epsilon J_x \subseteq [0,1]\}$ (41)

Figure 3 shows the overall structure of IT2-FLCs. Compared to T1-FLCs, the structure is quite similar. An IT2-FLC is one of the FLCs in the rule base, which is the main difference. Consequently, a type reducer is necessary to transform the inference engine's outputs from IT2-FLCs to T1-FLCs. To get a precise number, the IT2-FLC defuzzes the T1-FLCs (Milles *et al*., 2024).

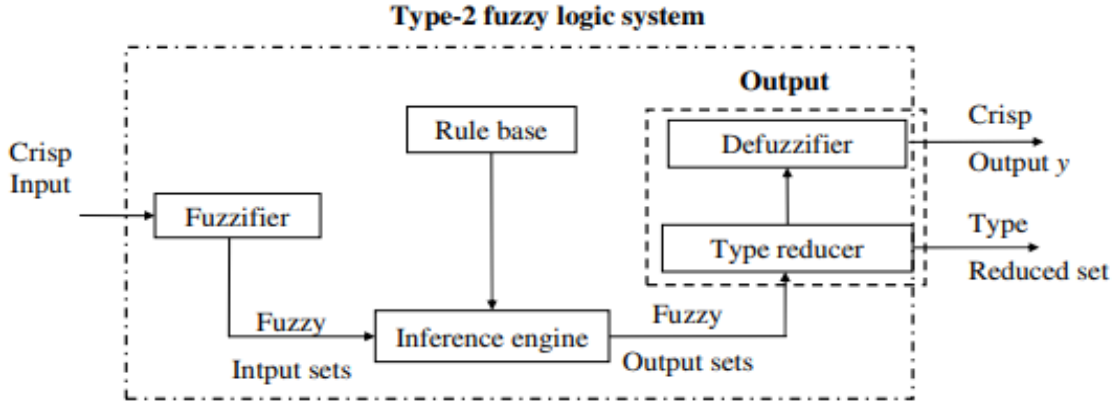

Figure 3- IT2- FLS configuration (Wu and Mendel, 2019).

Fuzzifier

The fuzzifier, similar to the process in a type-1 fuzzy logic system (T1-FLS), converts sharp input vectors $(e_1, e_2,..., e_n)^T$ into a type-2 fuzzy system $\tilde{A}_x$.

Rules

Here is an expression for the i[th] rule of an IT2-FLS:

$If e_1 is \bar{F}_1^i \ and If\ e_2\ is \bar{F}_2^i\ If\ e_n\ is \bar{F}_n^i, than y^i = \tilde{G}^i i=1,., M$ (42)

The inputs $x_1, x_2, \ldots\ldots\ldots, x_n$ are denoted by $\bar{F}_j^i$, which represents the IT2-FLS of the i[th] rule. The output of the IT2-FLS for the rule i is $\widetilde{G}^{\dot{1}}$, and M is the number of rules. The rule structure of an IT2-FLS closely resembles that of a T1-FLS, with the main distinction being the use of type-2 MFs instead of type-1 functions.

Inference Engine

The interval defined by the two extremes $\underline{f}^{\dot{1}}(x_i,\ldots..\ x_n)$ and $\bar{f}^{\dot{1}}(x_i,\ldots\ldots..,x_n)$is obtained by activating the i[th] rule $F^{\dot{1}}(x_i,\ldots.., x_n)$ in a fuzzy system of type-2 intervals that uses the minimum or product t-norm operations:

$$F^{\dot{l}}(x_i,\ldots\ldots..,x_n) = [\underline{f}^{\dot{i}}(x_i,\ldots\ldots..,x_n),\bar{f}^{\dot{l}}(x_i,\ldots\ldots..,x_n)] \equiv [\underline{f}^{\dot{i}}, \bar{f}^{\dot{l}}] \quad (43)$$

With $\underline{f}^{\dot{1}}$ and $\bar{f}^{\dot{l}}$ are given as:

$$\underline{f}^{\dot{i}} = \underline{\mu}_{F_1^i}(x_1) * \ldots..* \underline{\mu}_{F_n^i}(x_n) \quad (44)$$
$$\bar{f}^{\dot{l}} = \overline{\mu}_{F_1^i}(x_1) * \ldots\ldots..* \overline{\mu}_{F_n^i}(x_n)$$

Type Reducer

Following rule firing and inference, anIT2-FLS can be transformed into a T1FLS. Here, we review some methods for computing the centroid of an IT2-FLS based on the extension concept (Liang and Mendel, 2000). System A type-1 fuzzy centroid is:

$$c_A = \frac{\sum_{i=1}^{n} Z_i W_i}{\sum_{i=1}^{n} W_i} \quad (45)$$

Here, $Z_i$is a real number, W_i Here, Z_i is a real number, $W_i$is a real number between 0 and 1, and n is the number of discretized domains of A. The generalized centroid for IT2-FLS Ã may be determined by using the extension principle to T1-FLS $Z_i$and W_i, which have MFs $\mu_z(z_i)$ and $\mu_w(w_i)$ correspondingly.

$$\mathrm{GC}_{\tilde{\mathrm{A}}} = \int_{z_1 \epsilon Z_1} \ldots \int_{z_n \epsilon Z_n} \int_{w_1 \epsilon W1} \ldots \int_{w_n \epsilon W_n} \frac{[T_{i=1}^{n} \mu_z(z_i) * T_{i=1}^{n} \mu_w(z_i)]}{\frac{\sum_{i=1}^{n} Z_i W_i}{\sum_{i=1}^{n} W_i}} \quad (46)$$

Deffuzzifier

For the T1-FLC to provide legible output, the type-reduced set has to be defuzzified. The predominant approach is identifying the centroid of a collection that has been decreased in type. The centroid of the type-reduced set Y has been discretized into n points.

$$y_{ouptut}(x) = \frac{\sum_{i=1}^{n} y^i \mu(y^i)}{\sum_{i=1}^{m} \mu(y^i)} \quad (47)$$

To calculate the result, we can use the iterative Karnik-Mendel algorithm (Chen *et al*., 2024). Therefore, the outcome of an IT2-FLC defuzzification process is:

$$Y_{ouptut}(x) = \frac{y_l(x) + y_r(x)}{2} \quad (48)$$

With:

$$y_l(x) = \frac{\sum_{i=1}^{M} f_l^i y_l^i}{\sum_{i=1}^{M} f_l^i} \text{ and } y_r(x) = \frac{\sum_{i=1}^{M} f_r^i y_l^i}{\sum_{i=1}^{M} f_r^i} \quad (49)$$

Control of DFIG Using PFLC

The proposed structure is based on a nested loop, with the outer loop managing power control using the IT2-FLC approach. The observed states (stator and rotor currents, and speed) are used to transform the ID-PBC's inner loop into a dynamic feedback system. The suggested controller is shown in Figure 4.

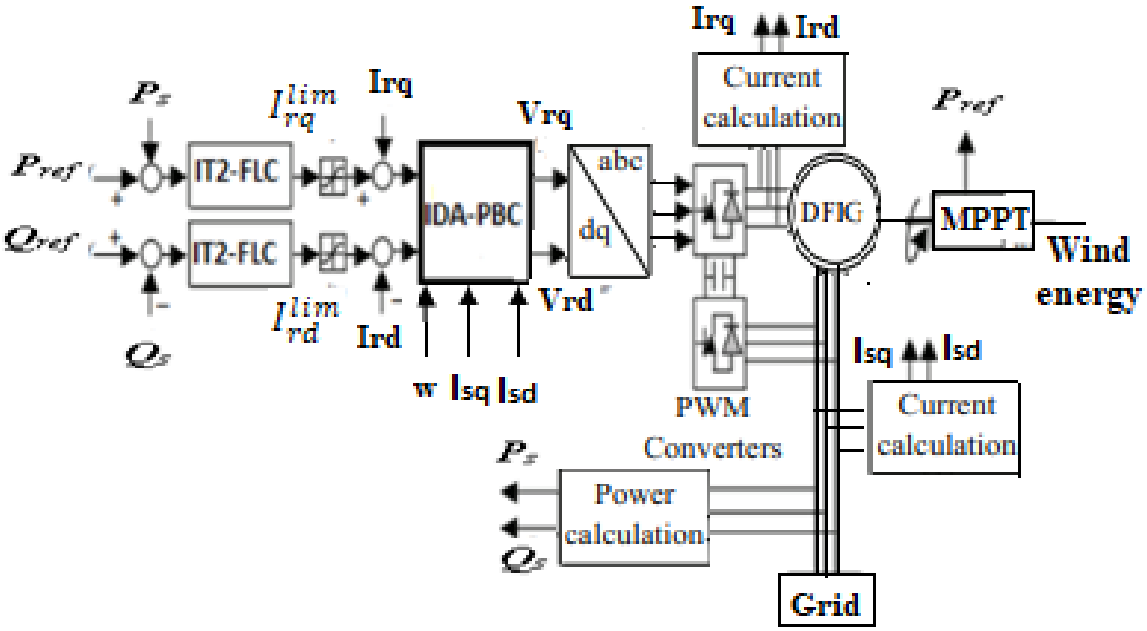

Figure 4- Proposed Structure with PFLC

Figure 5 shows the premise and consequence membership functions. Keep in mind that the domains of input and output discourse are scaled to the interval [-1, 1].

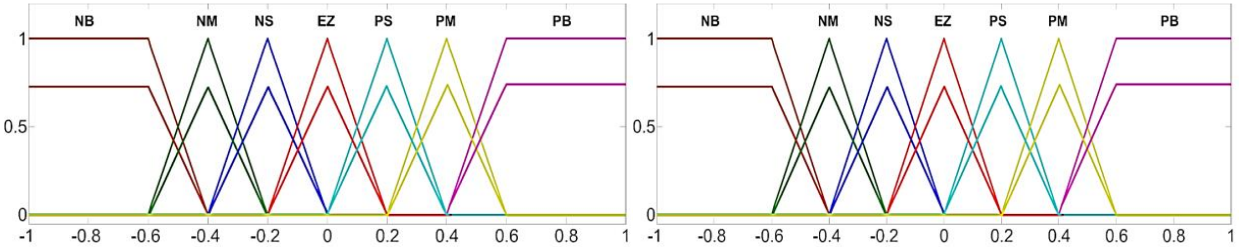

(a) **(b)**

Figure 5 - (a) TI2-FLC membership functions for input *e* and de (b). Membership function for output.

An inference matrix can represent the M rules given before. Table 1 compiles the fuzzy rules related to the controller in this work.

Table 1 - The fuzzy rules

e / *de*	**NB**	**NM**	**NS**	**ZE**	**PS**	**PM**	**PB**
NB	NB	NB	NB	NB	NM	NS	ZE
NM	NB	NB	NB	NM	NS	ZE	PS
NS	NB	NB	NM	NS	ZE	PS	PM
ZE	NB	NM	NS	ZE	PS	PM	PB
PS	NM	NS	ZE	PS	PM	PB	PB
PM	NS	ZE	PS	PM	PB	PB	PB
PB	EZ	PS	PM	PB	PB	PB	PB

Simulation results

This simulation segment uses a 10 KW generator linked to a 400V/50Hz grid. The system parameters are listed in Table 2. Two types of tests were administered: a tracking test, robust against fluctuations in machine parameters.

Table 2 - Parameters of the model.

Parameters	Value
Rated power	10 kW
Stator voltage	230/400 V
Frequency	50 Hz
Rs (Stator resistance)	0.455 Ω
Rr (Rotor resistance)	019 Ω
Ls (Stator inductance)	0.07 H
Lr (Rotor inductance)	0.0213 H
M (Mutual inductance)	0.034 H
P (Number of pole pairs)	2
$\boldsymbol{\rho}$ (Air density)	1.225 kg/m^3
R_b (Blade radius)	3.45m
Hm (Inertia constant)	2s
D (Damping coefficients)	0.01Nm.s/rad

First test

In this section, the techniques suggested for regulating the generator's efficacy are verified. Under optimal conditions, where no disturbances occur during operation, and without making any adjustments to the machine parameters.

The wind profile depicted in Figure .06 indicates that the WT will encounter an average speed of around 10 m/s. The derived power is significantly affected by even a minor variation in wind speed, as it is directly proportional to the cube of the wind speed. Evidently, the Ps exhibited a negative sign in this diagram, signifying that the DFIG generated and disseminated energy to the grid. The reactive power response was reduced to zero from 0 to 2.5 s to achieve unity power factor operation, as illustrated in Figure 7-(b). The performance achieved with the PFLC control is highly satisfactory, as demonstrated by the trajectory tracking and the extremely rapid convergence of the measured variables to the target reference, as illustrated in Figure 7. Utilizing this methodology facilitated the achievement of an impeccable decoupling between the stator power's two components.

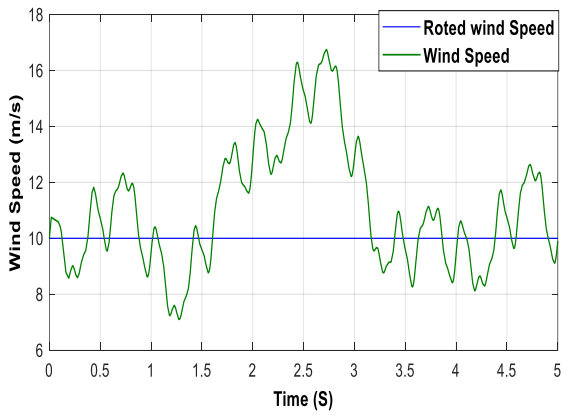

Figure 6 - Wind speed (V) profile.

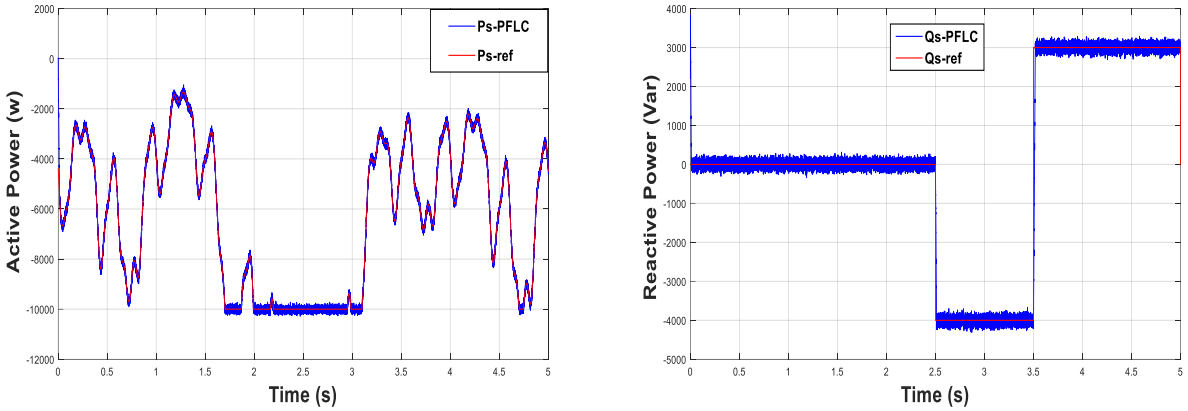

(a) **(b)**

Figure 7 - (a) Active power (*Ps*); (b) reactive power (*Qs*).

Figure 8 shows the components of the rotor current along the d- and q-axes, which correspond to the reactive and active power of the stator, respectively. Noteworthy, the rotor currents adhered to the reference trajectories, hence there was no overshooting.

Figure 9-(a) shows the sinusoidal waveform of the stator currents with a frequency of 50 Hz, varying with wind speed. However, the currents estimated in the rotor circuit are shown in Figure 9- (b) as sinusoidal waves, their frequency and magnitude changing based on slip or generator speed.

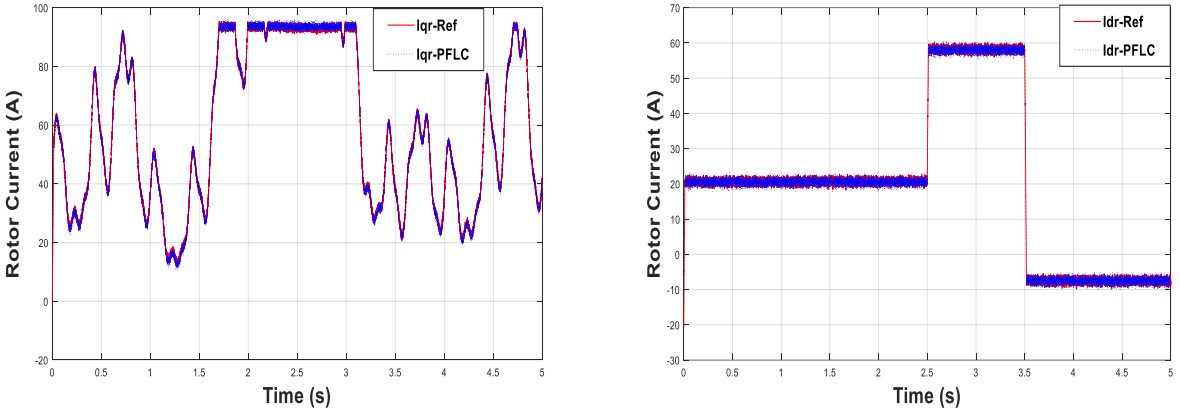

(a) **(b)**

Figure 8 - (a) rotor current (*Iqr*); (b) rotor current (*Idr*).

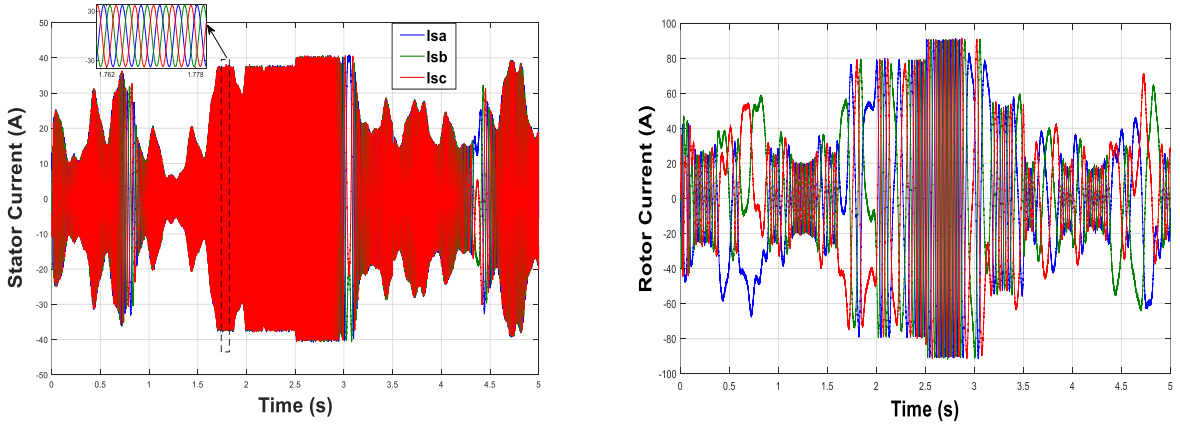

(a) **(b)**

Figure 9 - (a) stator current; (b) rotor current.

Robustness test

This section aims to assess and analyze the robustness and performance of the PFLC controller under adverse variations in control system parameters and wind speed disturbances. This test involves modifying the internal parameters of the generator to test the robustness of the PFLC unit and to evaluate the speed of its reaction to uncertainties. As a result, the stator and rotor resistance (R_r, R_s) are doubled. Moreover, the stator and rotor inductors (L_s, L_r) were adjusted to 30% of their nominal values, and M was reduced to 50% of its initial value.

The PFLC controller exhibited accurate performance, maintaining ps and qs closely aligned to the references without overshooting. Furthermore, the PFLC effectively minimized reactive and active power ripples. Simulations integrating passive-based control with an Interval type 2 fuzzy logic controller yielded remarkable results, including excellent reference tracking (time response and overshoot), disturbance sensitivity, and overall effectiveness.

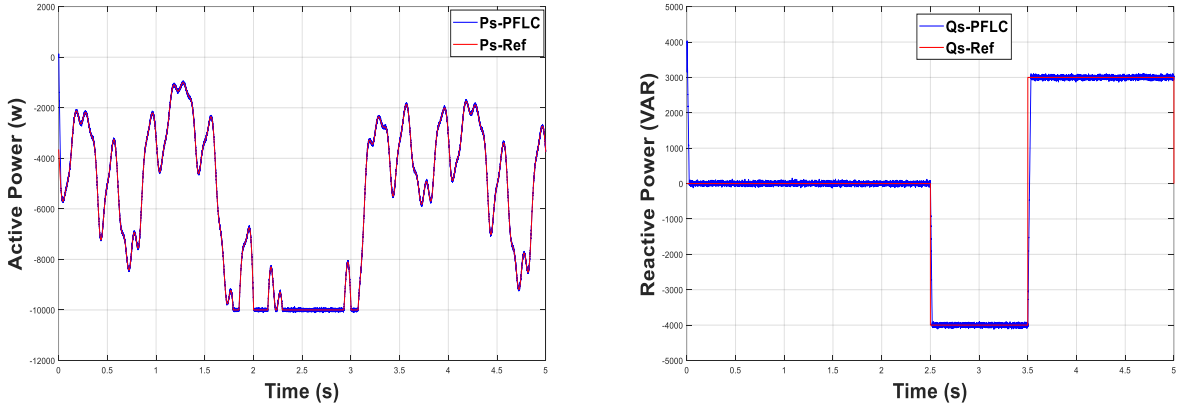

(a) **(b)**

Figure 10 - (a) Active power (Ps); (b) reactive power (Qs).

Conclusions

This study presents the results of our efforts to evaluate the efficacy of a DFIG's active and reactive powers via the use of hybrid passivity and fuzzy control. Following an explanation of the Doubly Fed Induction Generator (DFIG) with a fixed grid frequency and variable wind speed, we have developed a mathematical model of the DFIG's two-phase power. To manage the energetic electricity and the reactive electricity flows between the grid and the DFIG, the system was then subjected to two distinct scenarios that tested its resilience: disruptions caused by extremely high wind speeds and variations in system parameters. The IDA-PBC controller for a doubly-fed induction machine, combined with a fuzzy controller, has been implemented. The addition of a fuzzy logic component to the overall control system significantly improves the quality of active and reactive power, demonstrating excellent performance in reference tracking, perturbation sensitivity, and robustness against parameter variations.

Acknowledgement

The authors would like to sincerely thank the IRECOM Laboratory - University Djillali Liabs, Sidi Bel Abbes, Algeria for their support.

References

Acikgoz, H., Kececioglu, O., Gani, A., Tekin, M., & Sekkeli, M. (2017). Robust control of shunt active power filter using interval type-2 fuzzy logic controller for power quality improvement. *Tehnicki Vjesnik-Technical Gazette*, *24*. https://doi.org/10.17559/TV-20161213004749

Adeyanju, A. A. (2023). The Influence Of Rotor Separation On The Performance Of A Dual-Rotor Wind Turbine. *Journal of Namibian Studies: History Politics Culture*, *35*, 4684-4702. https://doi.org/10.59670/jns.v35i.4573

Amira, L., Tahar, B., & Abdelkrim, M. (2020, June). Sliding mode control of doubly-fed induction generator in wind energy conversion system. In *2020 8th International Conference on Smart Grid (icSmartGrid)* (pp. 96-100). IEEE. https://doi.org/ 10.1109/icSmartGrid49881.2020.9144778

Belkhier, Y., Achour, A., Bures, M., Ullah, N., Bajaj, M., Zawbaa, H. M., & Kamel, S. (2022). Interconnection and damping assignment passivity-based non-linear observer control for efficiency maximization of permanent magnet synchronous motor. *Energy Reports*, *8*, 1350-1361. https://doi.org/10.1016/j.egyr.2021.12.057

Chen, C., Wu, D., Garibaldi, J. M., John, R. I., Twycross, J., & Mendel, J. M. (2020). A comprehensive study of the efficiency of type-reduction algorithms. *IEEE Transactions on Fuzzy Systems*, *29*(6), 1556-1566. https://doi.org/ 10.1109/TFUZZ.2020.2981002

Doumi, M. H., Aissaoui, A., Tahour, A., Abid, M., & Tahir, K. (2016). Nonlinear integral backstepping control of wind energy conversion system based on a double-fed induction generator. *Przegląd Elektrotechniczny*, *92*(3), 130-135. https://doi.org /10.15199/48.2016.03.32

Heier, S. (2014). Grid integration of wind energy: onshore and offshore conversion systems. John Wiley & Sons.

Hemeyine, A. V., Abbou, A., Tidjani, N., Mokhlis, M., & Bakouri, A. (2020). Robust takagi sugeno fuzzy models control for a variable speed wind turbine based a DFI-generator. *International Journal of Intelligent Engineering and Systems*, *13*(3), 90-100. https://doi.org/10.22266/ijies2020.0630.09

Hichem, H., Abderrazak, T. A., Iliace, A., Bendelhoum, M. S., & Abdelkrim, B. (2023). A new robust SIDA-PBC approach to control a DFIGURE *Bulletin of Electrical Engineering and Informatics*, *12*(3), 1310-1317. https://doi.org/10.11591/eei.v12i3.2155

Kadri, A., Marzougui, H., Aouiti, A., & Bacha, F. (2020). Energy management and control strategy for a DFIG wind turbine/fuel cell hybrid system with supercapacitor storage system. *Energy*, *192*, 116518. https://doi.org/10.1016/j.energy.2019.116518

Kaloi, G. S., Baloch, M. H., Kumar, M., Soomro, D. M., Chauhdary, S. T., Memon, A. A., & Ishak, D. (2019). An LVRT scheme for grid connected DFIG based WECS using state feedback linearization control technique. *Electronics*, *8*(7), 777. https://doi.org/10.3390/electronics8070777

Khan, D., Ahmed Ansari, J., Aziz Khan, S., & Abrar, U. (2020). Power optimization control scheme for doubly fed induction generator used in wind turbine generators. *Inventions*, *5*(3), 40. https://doi.org/10.3390/inventions5030040

Kheir Saadaoui, B. B., Assas, O., & Khodja, M. A. (2019). Type-1 and type-2 fuzzy sets to control a nonlinear dynamic system. *Revue d'Intelligence Artificielle*, *33*(1), 1-7. https://doi.org/10.18280/ria.330101

Li, K., Zhang, X., & Han, Y. (2023). Robot path planning based on interval type-2 fuzzy controller optimized by an improved Aquila optimization algorithm. *IEEE Access*. https://doi.org/10.1109/ACCESS.2023.3323437

Liang, Q., & Mendel, J. M. (2000). Interval type-2 fuzzy logic systems: theory and design. IEEE Transactions on Fuzzy Systems, 8(5), 535-550. https://doi.org/10.1109/91.873577

Magaji, N., Mustafa, M. W. B., Lawan, A. U., Tukur, A., Abdullahi, I., & Marwan, M. (2022). Application of Type 2 Fuzzy for Maximum Power Point Tracker for Photovoltaic System. *Processes*, *10*(8), 1530. https://doi.org/10.3390/pr10081530

Milles, A., Merabet, E., Benbouhenni, H., Debdouche, N., & Colak, I. (2024). Robust control technique for wind turbine system with interval type-2 fuzzy strategy on a dual star induction generator. *Energy Reports*, *11*, 2715-2736. https://doi.org/10.1016/j.egyr.2024.01.060

Minka, I., Essadki, A., Mensou, S., & Nasser, T. (2019). Primary frequency control applied to the wind turbine based on the DFIG controlled by the ADRC. *International Journal of Power Electronics and Drive System*, *10*(2), 1049-1058. https://doi.org/ 10.11591/ijpeds

Mousa, H. H., Youssef, A. R., & Mohamed, E. E. (2020). Hybrid and adaptive sectors P&O MPPT algorithm based wind generation system. *Renewable Energy*, *145*, 1412-1429. https://doi.org/10.1016/j.renene.2019.06.078

Okedu, K. E., Al Tobi, M., & Al Araimi, S. (2021). Comparative study of the effects of machine parameters on DFIG and PMSG variable speed wind turbines during grid fault. *Frontiers in Energy Research*, *9*, 681443. https://doi.org/10.3389/fenrg.2021.681443

Sahri, Y., Tamalouzt, S., Lalouni Belaid, S., Bacha, S., Ullah, N., Ahamdi, A. A. A., & Alzaed, A. N. (2021). Advanced fuzzy 12 dtc control of doubly fed induction generator for optimal power extraction in wind turbine system under random wind conditions. *Sustainability*, *13*(21), 11593. https://doi.org/10.3390/su132111593

Saihi, L., Berbaoui, B., Djilali, L., & Boura, M. (2023). Sensorless passivity based control of doubly-fed induction generators in variable-speed wind turbine systems based on high gain observer. *Wind Engineering*, *47*(1), 86-103. https://doi.org/10.1177/0309524X221122531

Sanjuan, J. J. V., Flores, J. L., Mendoza, E. Y., & Tlaxcaltecatl, M. E. (2018, February). A sensorless passivity-based control for PMSM. In *2018 International Conference on Electronics, Communications and Computers (CONIELECOMP)* (pp. 86-91). IEEE. https://doi.org/10.1109/CONIELECOMP.2018.8327180

Scarabaggio, P., Grammatico, S., Carli, R., & Dotoli, M. (2021). Distributed demand side management with stochastic wind power forecasting. *IEEE Transactions on Control Systems Technology*, *30*(1), 97-112. https://doi.org/ 10.1109/TCST.2021.3056751

Shuaibu, M., Abubakar, A. S., & Shehu, A. F. (2021). Techniques for ensuring fault ride-through capability of grid connected dfig-based wind turbine systems: a review. *Nigerian Journal of Technological Development*, *18*(1), 39-46. https://doi.org/ 10.4314/njtd.v18i1.6

Wu, D., & Mendel, J. M. (2019). Recommendations on designing practical interval type-2 fuzzy systems. *Engineering Applications of Artificial Intelligence*, *85*, 182-193. https://doi.org/10.1016/j.engappai.2019.06.012

Xiong, L., Li, J., Li, P., Huang, S., Wang, Z., & Wang, J. (2021). Event triggered prescribed time convergence sliding mode control of DFIG with disturbance rejection capability. *International Journal of Electrical Power & Energy Systems*, *131*, 106970. https://doi.org/10.1016/j.ijepes.2021.106970

Yan, S. R., Dai, Y., Shakibjoo, A. D., Zhu, L., Taghizadeh, S., Ghaderpour, E., & Mohammadzadeh, A. (2024). A fractional-order multiple-model type-2 fuzzy control for interconnected power systems incorporating renewable energies and demand response. *Energy Reports*, *12*, 187-196. https://doi.org/10.1016/j.egyr.2024.06.018

Yang, B., Yu, T., Shu, H., Zhang, Y., Chen, J., Sang, Y., & Jiang, L. (2018). Passivity-based sliding-mode control design for optimal power extraction of a PMSG based variable speed wind turbine. *Renewable energy*, *119*, 577-589. https://doi.org/10.1016/j.renene.2017.12.047

Yin, M., Xu, Y., Shen, C., Liu, J., Dong, Z. Y., & Zou, Y. (2016). Turbine stability-constrained available wind power of variable speed wind turbines for active power control. *IEEE Transactions on Power Systems*, *32*(3), 2487-2488. https://doi.org/10.1109/TPWRS.2016.2605012